Implementation of stability-based transition model by means of transport equations

L. Pascal*, G. Delattre†, H. Deniau‡
ONERA/DMPE, Université de Toulouse - F-31055 Toulouse - France

G. Bégou§
ONERA/DAAA - Meudon - France

J. Cliquet¶
Airbus Opérations SAS - Toulouse - France

A natural laminar-turbulent transition model compatible with Computation Fluid Dynamics is presented. This model accounts for longitudinal transition mechanisms (i.e. Tollmien-Schlichting induced transition) thanks to systematic stability computation on similar boundary profiles from Mach zero to four both on adiabatic and isothermal wall. The model embeds as well the so-called "C1-criterion" for transverse transition mechanisms (i.e. cross-flow waves induced transition). The transition model is written under transport equations formalism and has been implemented in the solver *elsA* (ONERA-Airbus-Safran property). Validations are performed on three dimensional configurations and comparisons are shown against a database method for natural transition modeling and experiments.

I. Nomenclature

α = Angle of attack

γ = Intermittency

β_0 = Angle between the wall friction vector and the velocity vector at the boundary layer edge

Λ_2 = Pohlhausen parameter $\Lambda_2 = \frac{\theta^2}{\nu_e}\frac{dU_e}{ds}$

H = Boundary layer shape factor

M = Mach number

Re_{δ_1} = Displacement thickness based Reynolds number

Re_{δ_2} = Transverse displacement thickness based Reynolds number

Re_θ = Momentum thickness based Reynolds number

*Research Scientist, Multi-Physics and Energetics Department, lucas.pascal@onera.fr
†Research Scientist, Multi-Physics and Energetics Department
‡Research Scientist, Multi-Physics and Energetics Department
§Research Scientist, Department of Applied Aerodynamics
¶Engineer

n = Wall normal

s = Curvilinear abscissa

T_u = Turbulence level

Subscript(s)

e = Edge of the boundary layer

i = Incompressible

cr = Critical point of the boundary layer

tr = Transition location

∞ = Free-stream

II. Introduction

Accurate computation of transport aircraft drag strongly relies on natural laminar-turbulent transition prediction capabilities. As Computational Fluid Dynamics (CFD) is now a major component of industrial processes, it is necessary to develop accurate transition prediction techniques for RANS solvers both for aerodynamic performance prediction and for design of future laminar transport aircraft concepts.

The development of transition prediction methods compatible with CFD is a major research topic. A quite recent approach consists in using methods based on Partial Differential Equations (PDE). This approach consists in solving additional transport equations governing the dynamic of quantities that are related to transition process. The most famous PDE-based method is probably the "$\gamma - Re_\theta$" approach of Langtry and Menter [1] based on phenomenological reasoning. This method has demonstrated success on many configurations and has been extended to handle as well cross-flow transition [2]. The Amplification Factor Transport (AFT) method was derived more recently by Coder and Maughmer [3]. This promising method consists in writing under a transport equation the e^N method [4, 5] of Drela and Giles [6]. AFT method was recently extended to cross-flow transition by Xu et al. [7]. The $\gamma - Re_\theta$ and AFT methods are said to be "local" in the sense that the additional transport equations associated to transition only involve values available at RANS computational points. This property reduces much the implementation effort in a RANS solver.

As far as the *elsA* [8] RANS solver (property of Airbus-Safran-ONERA) is concerned, developments have been conducted to give access to non local variables (for instance integral boundary layer variables) at grid point. This feature has been used to implement the AHD criterion [9] evaluated along mesh lines [10] and the so-called "parabola method" [11] for transition prediction by means of transport equations [12].

This paper presents the implementation of the ONERA transition criteria (denoted AHD and C1) by means of transport equations and their comparison with the parabola method (embedded in a three dimensional boundary layer

equations solver). These criteria are presented in section III while section IV deals with their implementation in a RANS solver. Numerical results are presented in section V.

III. AHD/C1 transition criterion and parabola method for transition prediction

A. AHD criterion

The Arnal-Habiballah-Delcourt (AHD) criterion [9] was derived by performing linear stability analysis on two-dimensional incompressible similar profiles. The N-factor envelope is approximated by linear functions of the Pohlhausen parameter Λ_2:

$$N = a(\Lambda_2)(Re_\theta - Re_{\theta,cr}(\Lambda_2) + \Delta Re_{\theta,cr}(\Lambda_2)) \tag{1}$$

where:

$$\begin{cases} a(\Lambda_2) = \dfrac{2.4}{A}\exp(-B\Lambda_2) \\ \Delta Re_{\theta,cr} = -\dfrac{2.4}{a(\Lambda_2)}\left(\dfrac{8.43}{2.4} - \log(C) + D\right) \\ Re_{\theta,cr} = \exp\left(G/H_i^2 + E/H_i - F\right) \end{cases} \tag{2}$$

$Re_{\theta,cr}$ is the Reynolds number at the critical point, i.e. the location from which Tollmien-Schlichting instabilities start to grow. The dependency on Λ_2 is replaced by a dependency on H_i as there exists a biunivocal relationship between both. Due to the approximation error, $\Delta Re_{\theta,cr}$ is not zero.

To apply Eq. (1) on spatially evolving flows, Λ_2 is replaced by $\bar{\Lambda}_2$ which corresponds to its averaged value between the critical point of curvilinear abscissa s_{cr} and the current location of curvilinear abscissa s (measured along the streamline at the edge of the boundary layer):

$$\bar{\Lambda}_2 = \frac{1}{s - s_{cr}}\int_{s_cr}^{s} \Lambda_2(\xi)\mathrm{d}\xi.$$

By combining Eqs. (1) and the transition threshold N_T given by the Mack's law ($N_T = -2.4\ln(T_u) - 8.43$), the AHD transition criterion can be expressed as a threshold on Re_θ:

$$Re_{\theta,tr} = Re_{\theta,cr} + A\exp(B\bar{\Lambda}_2)\left(\ln(CT_u) - D\bar{\Lambda}_2\right) \ . \tag{3}$$

This criterion accounts for flow history through $\bar{\Lambda}_2$ and for receptivity through T_u. As this criterion is derived for natural transition, it should not be used for $T_u > 1\%$.

In its compressible extension [13], the variables A, B, C, D, E, F, G are function of M_e, the Mach number at the edge of the boundary layer. Moreover, this criterion accounts for effects of wall temperature [13, section V].

B. Gleyzes criterion

As the AHD criterion, Gleyzes criterion [14] was derived from systematic linear stability computations on similar boundary layer profiles. However, the boundary layer profiles correspond to separated profiles and the criterion models short bubbles transition. This criterion assumes that in the neighbourhood of and within the separated region, the growth rate of Tollmien-Schlichting waves is almost independent of the frequency. Therefore $\frac{dN}{dRe_\theta}$ depends only on the incompressible shape factor and is expressed as:

$$\frac{dN}{dRe_\theta} = \frac{-2.4}{\mathcal{B}(H_i)} \tag{4a}$$

$$\mathcal{B}(H_i) = \begin{cases} -\dfrac{162.11093}{H_i^{1.1}} & 3.36 < H_i \\ -73\exp\left(-1.56486(H_i - 3.02)\right) & 2.8 < H_i < 3.36 \\ -103\exp\left(-4.12633(H_i - 2.8)\right) & H_i < 2.8. \end{cases} \tag{4b}$$

1. Combine AHD and Gleyzes criteria

A "trick" is used to combine the AHD and Gleyzes criterion. Let s_{GL} be the curvilinear abscissa from which the Gleyzes criterion is triggered. Likewise, N_{GL}, $\bar{\Lambda}_{2,GL}$ and $Re_{\theta,GL}$ correspond to values at s_{GL}. According to Eq. (4b) The N-factor downstream of s_{GL} is simply:

$$N = N_{GL} + \int_{Re_{\theta,GL}}^{Re_\theta} \frac{-2.4}{\mathcal{B}(H_i)} \mathrm{d}R. \tag{5}$$

Let $\hat{N}$ be the N-factor according to the AHD criterion Eq. (1) corresponding to a fictitious flow where $\bar{\Lambda}_2$ remains $\bar{\Lambda}_{2,GL}$ downstream of s_{GL}:

$$\begin{aligned} \hat{N} &= a(\bar{\Lambda}_2)\left(Re_\theta - Re_{\theta,cr} + \Delta Re_{\theta,cr}(\bar{\Lambda}_2)\right) \\ &= N_{GL} + a(\bar{\Lambda}_{2,GL})(Re_\theta - Re_{\theta,GL}). \end{aligned} \tag{6}$$

Substituting N_{GL} from Eq. (6) into Eq. (5) yields:

$$N = a(\bar{\Lambda}_2)\left(Re_\theta - \hat{Re}_{\theta,cr} + \Delta Re_{\theta,cr}(\bar{\Lambda}_2)\right), \tag{7}$$

which corresponds to the standard form of the AHD criterion Eq. (1) where $Re_{\theta,cr}$ has been replaced by

$$\hat{Re}_{\theta,cr} = Re_{\theta,cr} + \int_{s_{GL}}^{s} \left(\frac{2.4}{a(\bar{\Lambda}_{2,GL})\mathcal{B}(H_i)} + 1\right) \frac{dRe_\theta}{ds} \mathrm{d}\xi \ . \tag{8}$$

.

Eq. (3) can be applied by replacing $Re_{\theta,cr}$ by $\hat{R}e_{\theta,cr}$. Following Ref. [6], $\frac{dRe_\theta}{ds}$ can be approximated by the following correlation:

$$\frac{dRe_\theta}{ds} = \frac{1}{2\theta}\left(0.058\frac{(H_i-4)^2}{H_i-1} + \frac{6.54H_i - 14.07}{H_i^2} - 0.068\right). \tag{9}$$

C. C1 criterion

The C1 criterion [15] is used to predict natural transition induced by cross-flow instabilities. This criterion defines the transition point as the location where the transverse incompressible displacement thickness Reynolds number $R_{\delta_{2i}}$ equals a threshold given by:

$$Re_{\delta_2,i,tr} = \begin{cases} 150 & H_i \leq 2.31 \\ \frac{300}{\pi}\arctan\left(\frac{0.106}{(H_i-2.3)^{2.052}}\right)\left(1+\frac{\gamma-1}{2}M_e^2\right) & 2.31 < H_i < 2.65 \end{cases} \tag{10}$$

(the criterion should not be applied for $H_i > 2.65$).

D. Parabola method

The so-called parabola method [11] is a database method which gives the growth-rate of longitudinal and transverse instabilities for a given velocity profile for a much lower computational effort than exact local linear stability analysis. As far as longitudinal instabilities are considered, the growth rate of a wave is given as a function of its angle ϕ, its frequency f and the following parameters of the boundary layer profile: the displacement thickness Reynolds number Re_{δ_1}, the incompressible shape factor H_i and the Mach number at the edge of the boundary layer M_e. The parabola method agrees well with exact local linear stability analysis [11, 16].

IV. Implementation in a CFD solver

A. Non local variables

Evaluating eqs. (3) or (10) requires the knowledge of boundary layer variables Re_θ, Re_{δ_2}, M_e, etc .... Contrary to the approaches presented in Ref. [1] or [3], the present method does not rely on correlations based on local variables. Non local variables are evaluated and made available at each cell point in *elsA* thanks to the fact that it is possible to: i) get for a cell in the volume the associated wall interface (if there is any) and ii) know which cells in the volume form the line normal to a given wall interface.

B. "Transition lines method"

An implementation of the AHD, Gleyzes and C1 criteria has first been proposed by Cliquet et al. [17]. It consists in assuming that streamlines at the boundary layer edge might be approximated by mesh lines. The implementation is denoted thereafter as "transition lines method". This method has been implemented in the *elsA* CFD solver and has shown good results on aircraft configuration [16], helicopter blades flow [18], etc ... However, this method requires some effort from the user as the latter is asked to prescribe the starting points of each transition line and what to do in case of transition computation failure.

C. Transport equations approach

To alleviate user effort and to account with higher fidelity for three dimensional geometries where streamlines directions might strongly differ from mesh lines, a new implementation of the AHD/C1 criteria has been derived. This implementation is based on transport equations which ensures that transition criteria are evaluated along streamlines. The method shares similarities with the method based on the ONERA parabola method derived by Bégou et al. [12].

In the following, the variables denoted ν_{cr}, ν_{tr} and ν_{GL} are nonlocal in the sense that are shared by all cells on a same wall normal. The term Γ_δ is introduced to restrain the influence of source term in a region near the walls and is defined by:

$$\Gamma_\delta = \exp\left(-\left(\frac{n}{4\delta}\right)^4\right). \tag{11}$$

1. AHD criterion

The first prerequisite to estimate the transition threshold $Re_{\theta,tr}$ following eq. (3) is to know the value of the critical Reynolds number downstream of the critical location. To answer this need, the transported variable $\widetilde{Re}_{\theta,cr}$ governed by:

$$\partial_t\left(\rho\widetilde{Re}_{\theta,cr}\right) + \nu_{cr}\nabla\cdot\left(\rho\widetilde{Re}_{\theta,cr}\underline{U}\right) = (1-\nu_{cr})\,\Gamma_{\widetilde{Re}_{\theta,cr}}\left(\widetilde{Re}_{\theta,cr} - Re_{\theta,cr}\right) \tag{12}$$

is introduced. ν_{cr} equals one where $Re_\theta \geq \widetilde{Re}_{\theta,cr,e}$ and zero elsewhere. As a consequence, as long as the boundary layer is not critical the source term forces $\widetilde{Re}_{\theta,cr}$ to equal $Re_{\theta,cr}$ and if the boundary layer becomes critical $\widetilde{Re}_{\theta,cr}$ is simply convected.

The second prerequisite is to compute the value of $\bar{\Lambda}_2$. To do so, a second transport equation is introduced (see section VI.B):

$$\partial_t\left(\rho\widetilde{\bar{\Lambda}}_2\right) + \nabla\cdot\left(\rho\widetilde{\bar{\Lambda}}_2\underline{U}\right) = \nu_{cr}\Gamma_\delta\frac{\rho||\underline{U}||}{\tilde{s}}\left(\Lambda_2 - \widetilde{\bar{\Lambda}}_2\right) + \Gamma_{\widetilde{\bar{\Lambda}}_2}(1-\nu_{cr})\Gamma_\delta\rho(\widetilde{\bar{\Lambda}}_2 - \Lambda_2) \tag{13}$$

where $\tilde{s}$ is an additional transported variable corresponding to the curvilinear abscissa measured from the critical point

(upstream of the critical point $\tilde{s}$ equals zero). $\tilde{s}$ is governed by (see section VI.A):

$$\partial_t\left(\rho\tilde{s}\right)+\nabla\cdot\left(\rho\tilde{s}\underline{U}\right)=\nu_{cr}\Gamma_\delta\rho||\underline{U}||-\Gamma_s\rho\left(1-\nu_{cr}\right)\tilde{s}\ . \tag{14}$$

The transition threshold on Re_θ given by Eq. (3) can then be evaluated from $\widetilde{\bar{\Lambda}}_{2,e}$ and $\widetilde{Re}_{\theta,cr,e}$ obtained by extracting $\widetilde{\bar{\Lambda}}_2$ and $\widetilde{Re}_{\theta,cr}$ at the edge of the boundary layer. A last equation is then added to set the intermittency of the transition point:

$$\partial_t\left(\rho\widetilde{\mathcal{I}}\right)+\nabla\cdot\left(\rho\widetilde{\mathcal{I}}\underline{U}\right)=\nu_{tr}\Gamma_\delta\rho||\underline{U}||-\Gamma_{\mathcal{I}}\rho\left(1-\nu_{tr}\right)\widetilde{\mathcal{I}}\ . \tag{15}$$

ν_{tr} equals one if $Re_\theta\geq Re_{\theta,tr}$ or $Re_{\delta_{2,i}}$ reaches $Re_{\delta_{2,i,tr}}$ (given by Eq. (10)). As a consequence $\widetilde{\mathcal{I}}$ corresponds to a curvilinear abscissa measured from the transition point (either induced by longitudinal or transverse instabilities).

The values of ν_{cr} and ν_{tr} are set to zero at the leading edge stagnation line and the variable $\widetilde{\mathcal{I}}$ is forced towards zero by the additional right hand side term:

$$-\Gamma_{\tilde{\mathcal{I}}}\widetilde{\mathcal{I}}. \tag{16}$$

The leading edge stagnation line is computed by following the method proposed by Kenwright et al. [19].

2. Coupling with turbulence models

The coupling with turbulence models is performed by multiplying the turbulence production terms and the Reynolds stress tensor by the intermittency γ. The latter is evaluated from the value of $\widetilde{\mathcal{I}}$ at the boundary layer edge $\widetilde{\mathcal{I}}_e$ according to (in the current implementation, the intermittency is set constant in the whole boundary layer profile):

$$\gamma(\widetilde{\mathcal{I}}_e)=1-\exp\left(-5\left(\frac{\widetilde{\mathcal{I}}_e}{l_{tr}}\right)^2\right). \tag{17}$$

Eq. (17) is derived from Refs. [20, Eqs. (1,6)]. At the current stage of development, the user is asked to prescribe the streamwise length l_{tr} of the transition region.

3. Gleyzes criterion

Following section III.B, the Gleyzes criterion is implemented by modifying the $\tilde{Re}_{\theta,cr}$ equation with an additional source term:

$$\nu_{GL}\Gamma_\delta\rho||U||\left(\frac{2.4}{a(\tilde{\bar{\Lambda}}_2)\mathcal{B}(H_i)}+1\right)\frac{dRe_\theta}{ds} \tag{18}$$

Where ν_{GL} equals one where $H_i>2.8$ (as in Ref. [10]) or $\beta_0>\pi/2$ (condition sufficient for a boundary layer profile to be separated) is zero elsewhere. $\dfrac{dRe_\theta}{ds}$ is given by Eq. (9). In order to make sure that $\bar{\Lambda}_2$ remains $\bar{\Lambda}_{2,GL}$ downstream of s_{GL}, the $\tilde{\bar{\Lambda}}_2$-equation and $\tilde{s}$-equation source terms are multiplied by $(1-\nu_{GL})$. Although it might be

already the case, ν_{cr} is set to one if ν_{GL} equals one.

4. C1 criterion

Due to the simplicity of C1 criterion, its implementation is quite straightforward. It consists in setting ν_{tr} to one in Eq. (15) if $\delta_{2,i}$ reaches the threshold given by Eq. (10).

V. Validations

Three three dimensional configurations have been chosen to validate the prediction method.

In sections V.A and V.C, validations are performed against results obtained with the 3C3D solver of ONERA which has been shown to give excellent results (see for instance Ref. [16]). The latter solves the boundary layer equations on three dimensional geometries. 3C3D takes as input the velocity at the edge of the boundary-layer, extracted here from full turbulent computation with *elsA* . It embeds the AHD/C1 transition criteria and the parabola method. Comparisons with 3C3D are useful i) to validate the implementation of the AHD/C1 transition criteria by means of transport equations ii) compare the transition location with linear stability theory (as explained in section III.D, parabola method shows excellent agreement with exact linear stability computations). Finally in section V.C validation are performed against experiments.

elsA computations are performed with a second order Roe spatial scheme and a backward Euler time scheme.

In the following, "transition line" denotes the location where the intermittency γ starts to grow.

A. M6 wing

This first validation case is the swept ONERA M6 wing. The flow conditions are taken from Ref [21]: $M_\infty = 0.262$, $Re = 3.5 \times 10^6$. Computations are performed for $\alpha = 5^o$. According to Schmitt and Cousteix [21], the turbulence level is $T_u = 0.2\%$. Even though experimental transition locations are given in Ref. [21], reproducing numerically this case is challenging since "one can assume that the application of the naphthalene sublimation technique has accelerated the transition" [22]. Moreover, wind-tunnels walls are not accounted for here. *elsA* computations are compared with 3C3D computations only performed with AHD and C1 criteria in order to validate the implementation of AHD and C1 criteria by means of transport equations in *elsA* . The turbulence model of Spalart and Allmaras [23] is here chosen. The mesh is composed of approximately 10×10^6 cells. The wing is meshed with 230 elements along the chord and about 60 elements along the span. In the laminar flow region, there are between 20 and 30 cells along the normal in the boundary layer following a geometric progression. Such refinement is known to be sufficient to catch quite accurately the stream-wise momentum thickness θ (necessary for AHD criterion) but might be insufficient to compute correctly the cross-flow displacement thickness δ_2 (necessary for C1 criterion).

The transition line predicted by *elsA* agrees quite well with 3C3D, see Figs. 1(a,b), even though boundary layer

refinement is quite coarse. As far as the suction side is considered, early transition is observed due to strong adverse pressure gradient (there is a leading-edge separation bubble from about 50% of the span up to the tip of the wing). Pressure side may be classified in three regions: at the root of the wing (approximately between 0% and 10% of the span) transition is triggered in *elsA* by C1 criterion. In 3C3D, transition is triggered by turbulent wedge contamination. At this stage of development, this mechanism is not accounted for by the model presented in this paper. The transition line is then quite flat until two third of the span. Transition is here triggered by C1 criterion. Finally, at the outer part of the wing, the transition location is again flat but transition is triggered by AHD criterion.

(a) (b)

Fig. 1 Intermittency contours (light and dark corresponds respectively to $\gamma = 0$ and $\gamma = 1$) at the suction (a) and pressure (b) sides. The black line depicts the transition location predicted by 3C3D by means of AHD/C1 transition criteria. Black squares depict transition by turbulent wedge in 3C3D. Flow is coming from left to right.

B. Nacelle transition prediction

While numerical validations of transition models in CFD are usually made on wings, numericals results on the XRF1 nacelle configuration of Airbus are shown in this section. A cut view of the geometry and of the surface mesh is shown in Fig. 2. The mesh was generated automatically and contains about 3×10^6 nodes. The nacelle is discretised by about 120 elements along the chord and 100 elements in the azimuthal direction. Laminar boundary layer profiles are discretised with ten to twenty elements in the wall normal direction. Such refinement is quite poor which does not ensure an accurate computation of boundary layer integral variables.

The turbulence level is set to $T_u = 0.1\%$ and the flow conditions are imposed with $\alpha = 1.1^{\circ}$ and $M_\infty \approx 0.6$. The Menter-SST turbulence model [24] is chosen.

The computed intermittency is plotted in Figs. 3(a,b) in the outer and inner sides of the nacelle. For the sake of visibility, both sides are "unrolled": the contours are shown in a plane (x, ψ) where $\psi \in [0, 2\pi]$ is defined as

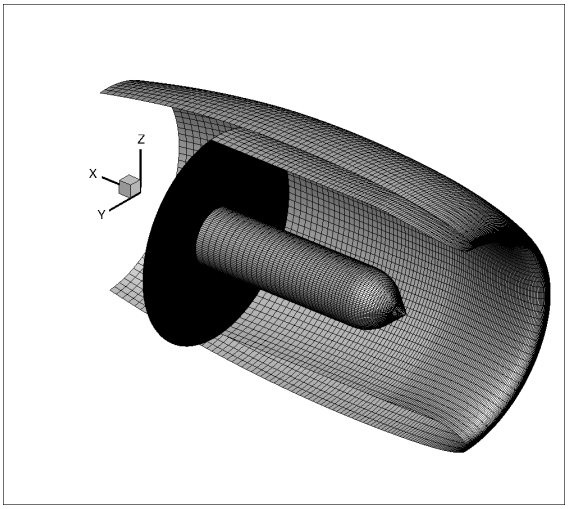

Fig. 2 Cut view of the XRF1 nacelle. Pressure boundary condition is imposed on the black surface.

$\tan(\psi) = z/y$ (see Fig. 2 for the definition of mesh axis). The transition line computed with the boundary layer equations solver 3C3D with the same transition criteria (AHD and C1) and with the parabola (only for Tollmien-Schliting instabilities) method. AHD criterion matches fairly well with parabola method. Moreover the implementation of the criteria by means of transport equations compares well with 3C3D solver. In the outer side, slight deviations are observed for $\psi \in [0, \pi]$ which corresponds to the upper part of the nacelle. As far as the inner side is considered, there are two small regions near $\psi = 0$ and $\psi = \pi$ where the transition location predicted by AHD and C1 criteria in 3C3D is slightly upstream because of C1 criterion. In these two regions, locally higher cross-flow velocity component is expected given the non zero angle of attack. The transition line obtained by means of the parabola method is not modified since only parabola method for Tollmien-Schlichting instabilities is here selected. In the CFD computation, $Re_{\delta_{2,i}}$ reaches 90% (respectively 98%) of $Re_{\delta_{2,i},tr}$ at the left side $\theta = 0$ (respectively at the right side $\theta = \pi$).

1. $\gamma - Re_\theta$ transition model

For the sake of comparison, the results obtained with the transition model of Langtry and Menter [1] are plotted on Fig. 4. Contours of incompressible shape factor are plotted, turbulent flow corresponds here to $H_i \approx 1.5$ and laminar flow to $H_i >\sim 2.2$. Fairly good comparison with parabola method is obtained even though it systematically anticipates the transition location, especially for $\psi \approx \pi/2$ at both the inner and upper sides.

C. Sickle wing

The last validation case is the sickle wing [25, 26]. This configuration is an interesting validation case since "the sickle-shaped planform with distinct kinks creates spanwise gradients, and the assumptions of linear local stability theory are therefore challenged" [25]. Kruse et al. [26] measured the transition location by means of infrared thermography.

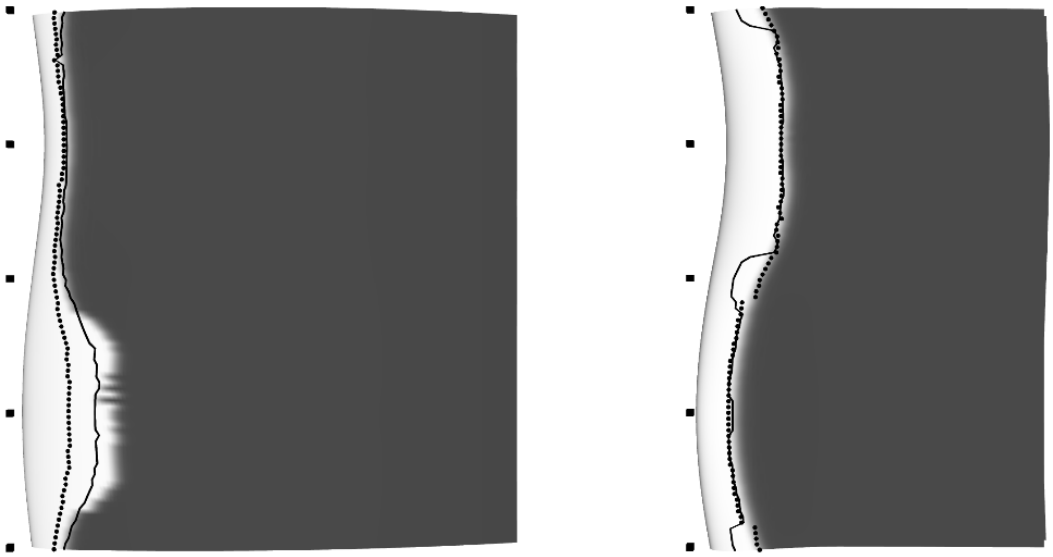

(a) (b)

Fig. 3 Intermittency contours computed with *elsA* by means of AHD and C1 criteria for transition prediction (light and dark corresponds respectively to $\gamma = 0$ and $\gamma = 1$) at the outer (a) and inner (b) sides of the nacelle. The black line (respectively the black symbols) depicts the transition location predicted by 3C3D by means of AHD/C1 transition criteria (respectively parabola method). Black squares depict $\psi \in \{0, \pi/2, \pi, 3\pi/2, 2\pi\}$. Flow is coming from left to right.

(a) (b)

Fig. 4 Incompressible shape factor H_i contours computed with *elsA* by means of $\gamma - Re_\theta$ model for transition prediction at the outer (a) and inner (b) sides of the nacelle. The black line (respectively the black symbols) depicts the transition location predicted by 3C3D by means of AHD/C1 transition criteria (respectively parabola method). Black squares depict $\psi \in \{0, \pi/2, \pi, 3\pi/2, 2\pi\}$. Flow is coming from left to right.

Table 1 Flow cases

	Re	α
Case A	2.75×10^6	-2.6^o
Case B	4.5×10^6	-2.6^o
Case C	4.5×10^6	-0.3^o
Case D	2.75×10^6	6.0^o

Computations are performed for four flow cases, see 1. Overset technique is used to mesh the wing within the wind tunnel. The mesh contains 48×10^6 cells among which 5.7×10^6 are in the overset block containing the wing. The latter is meshed with 230 elements along the chord on each side. The unswept segment at the root is meshed with 60 elements along the span while each swept segment is meshed with 120 elements along the span. For all four cases, between 40 and 60 cells are contained within the boundary layer thickness. Four all four computations, the flow is forced to be turbulent at the root of the wing on both sides.

The computed intermittency is plotted on Figures 5, 6, 7 and 8 together with the experimentally measured transition locations.

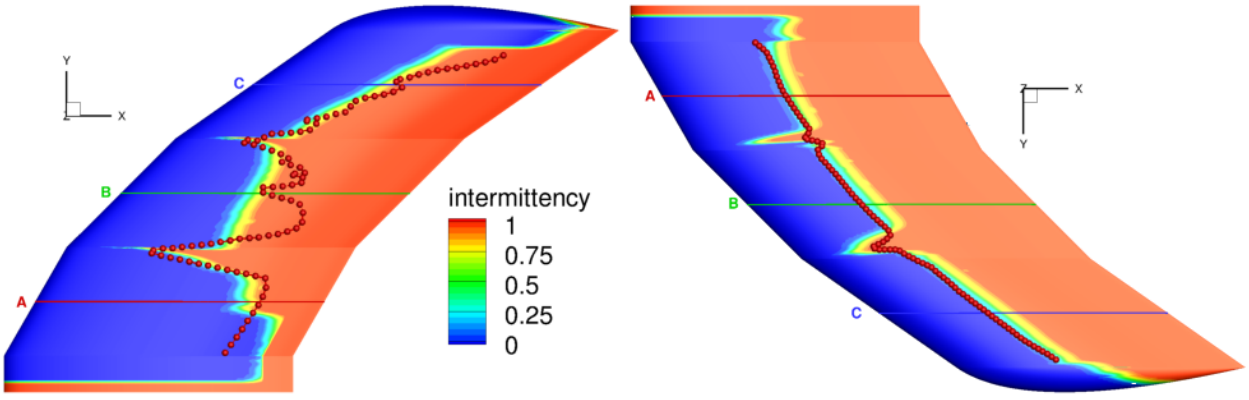

Fig. 5 Sickle wing, case A - Contours of γ compared to the experimentally measured transition locations at the suction (left) and pressure (right) sides.

For case A (Figure 5), very good transition agreement is obtained on the pressure side, where transition is mostly due to longitudinal mechanisms. The model is even able to reproduce the behaviour observed at the kinks where transition is induced by cross-flow mechanism. As far as the upper side is concerned, the model agrees well with the experiments. At the root, the tip of the wing and around section B, the model is not able to reproduce the experimental results. Except at the root and at the tip of the wing, transition is induced by cross-flow instabilities.

On case B (Figure 6) and for both sides, transition is moslty triggered by the C1 criterion except at the root of the wing (flat region below span section A). The computed transition location agrees quite well with the experiments.

Similarly to case B, transition is triggered by AHD criterion at the root of wing (flat region below span section A)

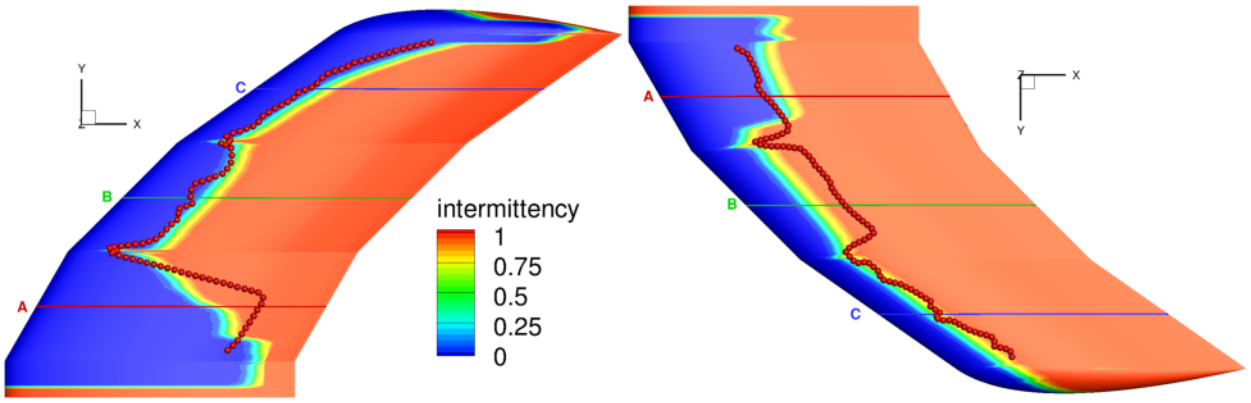

Fig. 6 Sickle wing, case B - Contours of γ compared to the experimentally measured transition locations at the suction (left) and pressure (right) sides.

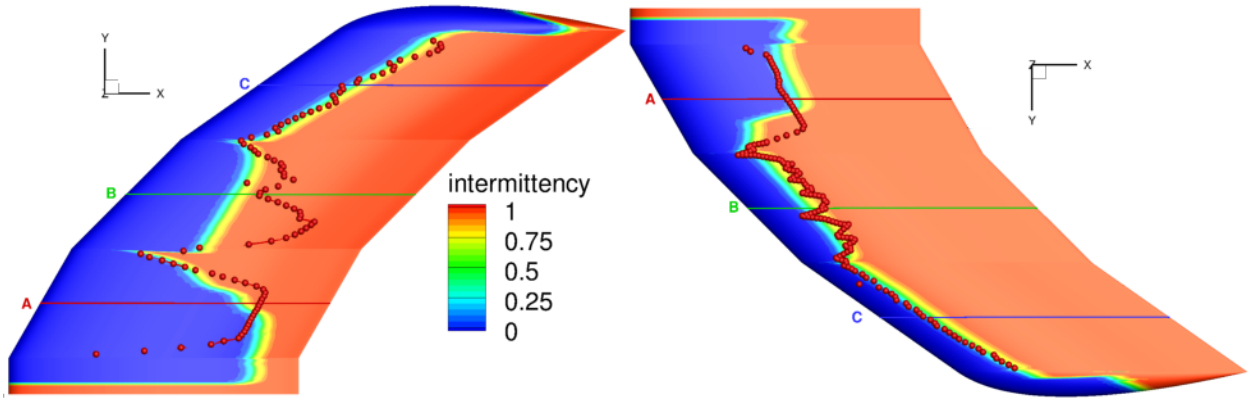

Fig. 7 Sickle wing, case C - Contours of γ compared to the experimentally measured transition locations at the suction (left) and pressure (right) sides.

on both sides of case C (Figure 7). Elsewhere transition is triggered by C1 criterion. The model yields quite good agreement with experiments. As observed already on case A, the model is not able to reproduce the trend measured at the suction side near the span section B.

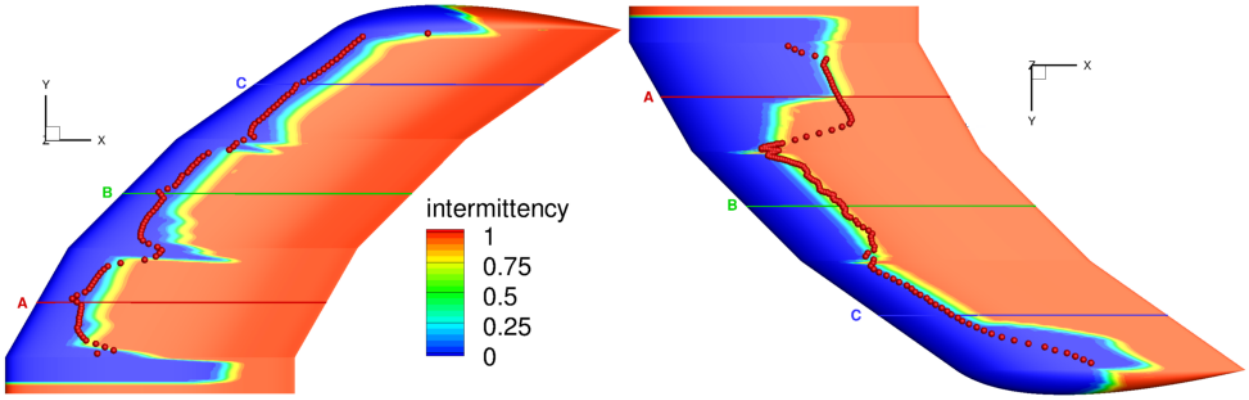

Fig. 8 Sickle wing, case D - Contours of γ compared to the experimentally measured transition locations at the suction (left) and pressure (right) sides.

The transition model yields a quite good agreement with the experiments on case D (see Figure 8). Compared to the experiments, the model slightly delays the transition location on the suction side, especially near the first kink. While on the suction side transition is only triggered by AHD criterion, the flat transition line around the span section B on the pressure side is due to the C1 criterion. Above the span section C on the pressure side, the model does not agree very well with the transition location experimentally measured.

VI. Conclusion

An implementation of the stability based AHD criterion by means of transport equations is presented. This criterion, valid for Mach number up to $M = 4$ and for heated and cold wall, is combined with C1 and Gleyzes criteria to account for cross-flow transition and transition in separation bubbles.

The implementation by means of transport equations and the accuracy of the model were validated by comparing with results obtained with the boundary layer equations solver `3C3D` on the M6 wing and on the XRF1 nacelle. Comparisons with experiments were performed for four flow cases on the sickle wing geometry. The obtained results ranged from quite good to excellent agreement with experiments.

The method may be applied at early design stages as good agreement with linear stability theory was observed even on poorly refined mesh generated automatically. Transition prediction in CFD matching closely exact local linear stability computations can be obtained thanks to the method of Bégou et al. [12] for higher computational cost. This latter method complements well with the method presented in this paper as it can be used in more advanced design stages.

Acknowledgement

Antoine Dumont (ONERA/DAAA) is gratefully acknowledged for providing the M6 wing mesh.

Andreas Krumbein (DLR Göttingen) and Martin Kruse (DLR Braunschweig) are gratefully acknowledged for providing the sickle wing CAD and the experimentally measured transition locations.

Appendix

In the following sections, we show that solving Eqs.(14) and (13) corresponds to computing s and $\bar{\Lambda}_2$ by means of transport equations.

A. Transport equation compute s

Let s be the curvilinear abscissa at $(\underline{x},t)$. At $t+\Delta t$, the new location is $\underline{x}+\Delta\underline{x} = \underline{x}+\underline{U}\Delta t$ and the curvilinear abscissa is $s(\underline{x}+\Delta\underline{x},t+\Delta t) = s(\underline{x},t)+\Delta t\|\underline{U}\|$. Taylor expansion yields:

$$s(\underline{x}+\Delta\underline{x},t+\Delta t) = s(\underline{x},t)+\nabla s\cdot\underline{U}\Delta t+\partial_t s\Delta t \tag{19}$$

which implies that:

$$\partial_t s+\nabla s\cdot\underline{U} = \|\underline{U}\|. \tag{20}$$

Combining Eq. (20) with the continuity equation of the Navier-Stokes equation yields:

$$\partial_t(\rho s)+\nabla(\rho s)\cdot\underline{U} = \rho\|\underline{U}\|. \tag{21}$$

B. Transport equation to compute $\bar{\Lambda}_2$

Let $\bar{\Lambda}_2$ be the average Pohlhausen value at $(\underline{x},t)$. At $t+\Delta t$, the new location is $\underline{x}+\Delta\underline{x} = \underline{x}+\underline{U}\Delta t$ and the average Pohlhausen value is

$$\bar{\Lambda}_2(\underline{x}+\Delta\underline{x},t+\Delta t) = \frac{s\bar{\Lambda}_2(\underline{x},t)+\Delta t\|\underline{U}\|\Lambda_2}{s(\underline{x}+\Delta\underline{x},t+\Delta t)} \tag{22}$$

.

Taylor expansion yields:

$$\bar{\Lambda}_2(\underline{x},t)+\nabla\bar{\Lambda}_2\cdot\underline{U}\Delta t+\partial_t\bar{\Lambda}_2\Delta t = \frac{s\bar{\Lambda}_2(\underline{x},t)+\Delta t\|\underline{U}\|\Lambda_2}{s(\underline{x},t)+\nabla s\cdot\underline{U}\Delta t+\partial_t s\Delta t} \tag{23}$$

which can be combined with Eq. (20):

$$\left(\bar{\Lambda}_2(\underline{x},t)+\nabla\bar{\Lambda}_2\cdot\underline{U}\Delta t+\partial_t\bar{\Lambda}_2\Delta t\right)\left(s(\underline{x},t)+\Delta t\|\underline{U}\|\right) = s\bar{\Lambda}_2(\underline{x},t)+\Delta t\|\underline{U}\|\Lambda_2 \tag{24}$$

Neglecting $O(\Delta t^2)$ terms yields:

$$\partial_t \bar{\Lambda}_2 + \nabla \bar{\Lambda}_2 \cdot \underline{U} = \frac{\|\underline{U}\|}{s} \left(\Lambda_2 - \bar{\Lambda}_2 \right). \tag{25}$$

Combining Eq. (25) with the continuity equation of the Navier-Stokes equation yields:

$$\partial_t (\rho \bar{\Lambda}_2) + \nabla (\rho \bar{\Lambda}_2) \cdot \underline{U} = \rho \frac{\|\underline{U}\|}{s} \left(\Lambda_2 - \bar{\Lambda}_2 \right). \tag{26}$$

References

[1] Langtry, R. B., and Menter, F. R., "Correlation-Based Transition Modeling for Unstructured Parallelized Computational Fluid Dynamics Codes," *AIAA Journal*, Vol. 47, No. 12, 2009, p. 2894–2906.

[2] Grabe, C., Shengyang, N., and Krumbein, A., "Transport Modeling for the Prediction of Crossflow Transition," *AIAA Journal*, Vol. 56, No. 8, 2018, pp. 3167–3178.

[3] Coder, J. G., and Maughmer, M. D., "Computational Fluid Dynamics Compatible Transition Modeling Using an Amplification Factor Transport Equation," *AIAA Journal*, Vol. 52, No. 11, 2014, p. 2506–2512.

[4] Van Ingen, J. L., "A suggested semi-empirical method for the calculation of the boundary layer transition region," Tech. Rep. VTH-74, Dept. of Aerospace Engineering, Delft Univ. of Technology, 1956.

[5] Smith, A. M. O., and Gamberoni, N., "Transition, pressure gradient, and stability theory," Tech. Rep. ES-26388, Douglas Aircraft, 1956.

[6] Drela, M., and Giles, M. B., "Viscous-inviscid analysis of transonic and low Reynolds number airfoils," *AIAA journal*, Vol. 25, No. 10, 1987, pp. 1347–1355.

[7] Xu, J., Han, X., Qiao, L., Bai, J., and Zhang, Y., "Fully Local Amplification Factor Transport Equation for Stationary Crossflow Instabilities," *AIAA Journal*, 2019, pp. 1–12.

[8] Cambier, L., Heib, S., and Plot, S., "The Onera elsA CFD software: input from research and feedback from industry," *Mechanics & Industry*, Vol. 14, No. 3, 2013, pp. 159–174.

[9] Arnal, D., "Transition prediction in transonic flow," *Symposium Transsonicum III*, Springer, 1989, pp. 253–262.

[10] Perraud, J., Deniau, H., and Casalis, G., "Overview of transition prediction tools in the elsA software," *ECCOMAS*, 2014.

[11] Perraud, J., Arnal, D., Casalis, G., Archambaud, J.-P., and Donelli, R., "Automatic transition predictions using simplified methods," *AIAA journal*, Vol. 47, No. 11, 2009, pp. 2676–2684.

[12] Bégou, G., Deniau, H., Vermeersch, O., and Casalis, G., "Database Approach for Laminar-Turbulent Transition Prediction: Navier–Stokes Compatible Reformulation," *AIAA Journal*, 2017, pp. 3648–3660.

[13] Perraud, J., and Durant, A., "Stability-Based Mach Zero to Four Longitudinal Transition Prediction Criterion," *Journal of Spacecraft and Rockets*, 2016, pp. 730–742.

[14] Gleyzes, C., Cousteix, J., and Bonnet, J. L., "Theoretical and experimental study of low Reynolds number transitional separation bubbles," *Conference on Low Reynolds Number Airfoil Aerodynamics, Notre Dame, IN*, 1985, pp. 137–152.

[15] Arnal, D., Habiballah, M., and Coustols, E., "Théorie de l'instabilité laminaire et critères de transition en écoulement bi et tridimensionnel," *La Recherche Aérospatiale*, Vol. 2, 1984, pp. 125–143.

[16] Hue, D., Vermeersch, O., Duchemin, J., Colin, O., and Tran, D., "Wind-Tunnel and CFD Investigations Focused on Transition and Performance Predictions of Laminar Wings," *AIAA Journal*, Vol. 56, No. 1, 2018, pp. 132–145.

[17] Cliquet, J., Houdeville, R., and Arnal, D., "Application of Laminar-Turbulent Transition Criteria in Navier-Stokes Computations," *AIAA Journal*, Vol. 46, No. 5, 2008, pp. 1182–1190.

[18] Richez, F., Nazarians, A., and Lienard, C., "Assessment of laminar-turbulent transition modeling methods for the prediction of helicopter rotor performance," *43rd European Rotorcraft Forum*, 2017.

[19] Kenwright, D. N., Henze, C., and Levit, C., "Feature extraction of separation and attachment lines," *Visualization and Computer Graphics, IEEE Transactions on visualization and computer graphics*, Vol. 5, No. 2, 1999, pp. 135–144.

[20] Stock, H. W., and Haase, W., "Navier-Stokes Airfoil Computations with e Transition Prediction Including Transitional Flow Regions," *AIAA journal*, Vol. 38, No. 11, 2000, pp. 2059–2066.

[21] Schmitt, V., and Cousteix, J., "Étude de la couche limite tridimensionnelle sur une aile en flèche," Tech. Rep. 14/1713, ONERA, 1975.

[22] Krumbein, A. M., "Automatic Transition Prediction and Application to Three-Dimensional Wing Configurations," *Journal of Aircraft*, Vol. 44, No. 1, 2007, pp. 119–133.

[23] Spalart, P., and Allmaras, S. R., "A One-Equation Turbulence Model for Aerodynamic Flows," *AIAA*, Vol. 439, No. 1, 1992.

[24] Menter, F. R., "Two-equation eddy-viscosity turbulence models for engineering applications," *AIAA journal*, Vol. 32, No. 8, 1994, pp. 1598–1605.

[25] Petzold, R., and Radespiel, R., "Transition on a Wing with Spanwise Varying Crossflow and Linear Stability Analysis," *AIAA Journal*, Vol. 53, No. 2, 2015, pp. 321–335.

[26] Kruse, M., Munoz, F., Radespiel, R., and Grabe, C., "Transition Prediction Results for Sickle Wing and NLF(1)-0416 Test Cases," *2018 AIAA Aerospace Sciences Meeting*, American Institute of Aeronautics and Astronautics, 2018.